Cooperative Path-Following for Multirotor UAVs with a Suspended Payload

Kristian Klausen*, Thor I. Fossen†, Tor Arne Johansen‡, A. Pedro Aguiar§
*†‡Centre for Autonomous Marine Operations and Systems (AMOS)
Department of Engineering Cybernetics,
Norwegian University of Science and Technology (NTNU), 7491 Trondheim, Norway
§Research Center for Systems and Technologies, Faculty of Engineering, University of Porto.

***Abstract*—In this paper, we present a cooperative control strategy for a team of multirotor type UAVs to lift a suspended payload. The interconnected system is modeled by the Udwadia-Kalaba equations of constrained motion. A robust path-following controller is developed for each vehicle in the system, and coordination is achieved through synchronization of the path parameterization. Stability of the interconnected system consisting of a network of local path-following controllers is analyzed. Results are verified by numerical simulations.**

I. Introduction

In the recent years, the usability of Unmanned Aerial Vehicles (UAVs) has increased proportionally with availability, technology maturity and declining cost of inertial sensors. This holds especially true for multirotor-type UAVs, which now are used for several commercial and consumer applications. Most of these multirotors are small (< 2.5 kg) and relatively cheap. In some regions of the world, the total take-off weight of a vehicle is important to keep below such limits due to aviation guidelines.

This paper considers the use of multirotor UAVs to transport a suspended payload. This load can be a variety of things, such as cargo transportation or sensor deployment. Due to the inherent capacity limitations of small multirotor UAVs, we illustrate how a team of UAVs can cooperatively transport a single payload to distribute and minimize the load on each vehicle, thus increasing the total lift capacity and operation time.

Similar problems are addressed for scale helicopters in [1], which were also validated in experiments. [2] considers motion planning and control for a team of indoor multirotors to manipulate a suspended payload, and [3] utilizes geometric control to generate coordinate-free controllers to control a suspended load in 6 degrees of freedom (DOF). In addition to distributed control, this paper also considers synchronization between the vehicles in the mission over a communication network. Fundamental consensus algorithms for synchronization are discussed in detail in [4], utilizing graph theory to create distributed control laws under communication constraints. Passivity-based approaches are discussed in [5], [6]. See also [7] and references therein.

This work was partially supported by the Research Council of Norway through its Centers of Excellence funding scheme, grant number 223254 (Centre for Autonomous Marine Operations and Systems).

In [8], the authors introduce a method to solve the formation maneuvering problem. By solving individual maneuvering problems ([9], [10]), it is shown that by distributing and synchronizing their path parameterization variable, the formation problem can be solved. Utilizing graph theory ([11]), a similar framework (coordinated path-following) is introduced in [12] and applied to a team of under-actuated autonomous underwater vehicles. In [13] and [14], the coordinated path-following (CPF) problem is addressed in the presence of time delays and discrete logic-based communications, respectively.

This paper applies the results from the above citations to the team of multirotors transporting the suspended payload. By synchronizing each UAV along a certain path, the position of the suspended load can be manipulated.

The paper is organized as follows. First, the problem is described in more detail. The dynamical system is modeled using a combination of Newton-Euler mechanics for each individual vehicle, while the interconnected system with dynamical constraints imposed by transportation wires is modeled by the Fundamental Equation [15]. In Section IV, a non-linear path-following controller is designed for the multirotors by the back-stepping technique. Further in Section V, a controller to synchronize the vehicles along the path using communication links is presented. Section VI illustrates an algorithm for spatial path generation for each vehicle, that minimizes the load drag variation among the multirotors as they move along the desired load path. A speed profile is designed next, followed by numerical simulations in Section VIII.

II. Problem Statement

Inspired by [12], we design the overall controller in two parts. First, a local controller that solves the *path-following problem* is employed on each vehicle:

Definition 1. Path-following problem ([12]):
Let $\mathbf{p}_{d_i}(\gamma) \in \mathbb{R}^3$ be a desired path parameterized by a continuous variable $\gamma_i \in \mathbb{R}$, and $v_L(\gamma_i) \in \mathbb{R}$ a desired reference speed for vehicle i. Design feedback control laws for $\boldsymbol{\tau}_i$, such that all the closed-loop signals are bounded, the position of the vehicle converges to and remains inside a tube centered around the desired path, and the vehicle travels at a

desired speed assignment v_L, that is, $\dot{\gamma} - v_L \to 0$ as $t \to \infty$.

The path-following controller is designed in such a way, that it can take an extra input, $\tilde{v}_i$, as a coordination variable to speed up or slow down along the path, to synchronize its position along the path with the other vehicles. This is the *coordination problem*:

Definition 2. Coordination problem ([12]):
For each vehicle $i \in \mathcal{I} := 1, \ldots, n$ derive a control law for the speed command as a function of γ_i and γ_j, $j \in \mathcal{N}$, such that $\gamma_i - \gamma_j, \forall i, j \in \mathcal{I}$ approach zero as $t \to \infty$ and the formation travels at an assigned speed v_L, that is, $|\dot{\gamma}_i - v_L|$ tends to zero.

The coordinated path-following (CPF) problem is the combination of the two previous stated problems. An overview of the control architecture can be seen in Figure 1.

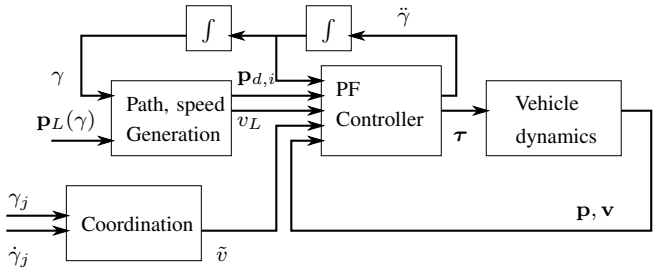

Fig. 1. An overview of the controller structure.

III. Dynamic modeling

In this section, a dynamical model of a single UAV is first presented. This is a well-studied system in the literature, and the presentation is thus quite brief. Next, we illustrate how the equations of Udwadia and Kalaba [15] can be used to find the forces of constraint acting on each vehicle due to the interconnecting wires. This is based on the work in [16].

Let the NED frame $\{n\}$ be an inertial frame. The position of each UAV in this inertial frame is given by $\mathbf{p}_i \in \mathbb{R}^3$. Further, let $\{b_i\}$ be a body-aligned frame at UAV i, whose orientation wrt. $\{n\}$ is given by the transformation matrix $\mathbf{R}^n_{b,i} \in \mathcal{SO}^3$. Thus, the kinematics are given by

$$\dot{\mathbf{p}}_i = \mathbf{R}^n_{b,i}\mathbf{v} \tag{1}$$

$$\dot{\mathbf{R}}^n_{b,i} = \mathbf{S}(\boldsymbol{\omega}^n_{b,i})\mathbf{R}^n_{b,i} \tag{2}$$

where $\mathbf{v} \in \mathbb{R}^3$ is the translational velocity in $\{b_i\}$, $\boldsymbol{\omega}^n_{b,i}$ is the rotational velocity of $\{b_i\}$ with respect to $\{n\}$, and $\mathbf{S}(\cdot)$ is the skew-symmetric matrix operator defined by

$$\mathbf{S}(\lambda) := \begin{bmatrix} 0 & -\lambda_3 & \lambda_2 \\ \lambda_3 & 0 & -\lambda_1 \\ -\lambda_2 & \lambda_1 & 0 \end{bmatrix} \tag{3}$$

for $\lambda \in \mathbb{R}^3$.

The kinetics are given from standard Newton-Euler rigid-body dynamics:

$$\mathbf{M}_i\dot{\mathbf{v}}_i = -\mathbf{S}(\boldsymbol{\omega})\mathbf{M}_i + \boldsymbol{\tau}_{a,i} + \Pi\tau_{c,i} + \mathbf{g}_i + \boldsymbol{\tau}_{L,i} \tag{4}$$

$$\mathbf{J}_i\dot{\boldsymbol{\omega}}^n_{b,i} = \mathbf{S}(\mathbf{J}_i\boldsymbol{\omega}^n_{b,i})\boldsymbol{\omega}^n_{b,i} + \boldsymbol{\tau}_{M,i} \tag{5}$$

where $\mathbf{M}_i > 0, \in \mathbb{R}^{3\times3}$ is the mass matrix of the vehicle, and $\mathbf{J}_i > 0$ its inertia dyadic in the vehicle body fixed frame. As a multirotor is only capable of producing translational force along its z-axis, we have $\Pi = [0, 0, 1]^{\mathrm{T}}$ and the control force $\tau_{c,i} \in \mathbb{R}$. The effect of gravity is $\mathbf{g}_i = \mathbf{R}^n_{b,i}[0, 0, m_i g]^{\mathrm{T}}$. $\boldsymbol{\tau}_{a,i} \in \mathbb{R}^3$ encompasses all aerodynamical forces acting on the body. $\boldsymbol{\tau}_{M,i} \in \mathbb{R}^3$ represents control momentum. $\boldsymbol{\tau}_{L,i} \in \mathbb{R}^3$ are the forces of constraint from the suspended payload.

In this paper, we consider the suspended payload as a point-mass with position $\mathbf{p}_l$ and mass m_l, which gives the dynamics:

$$m_l\ddot{\mathbf{p}}_l = \begin{bmatrix} 0 \\ 0 \\ m_l g \end{bmatrix} - \sum_{i=0}^{N} \boldsymbol{\tau}_{L,i} \tag{6}$$

Next, we utilize the results in [17] to find the forces of constraint $\boldsymbol{\tau}_{L,i}$.

A. Multi-body modeling

This section is based on the work by [16] and [17].

Consider N multirotors, connected by N wires from the body centre of gravity to a suspended load. The goal is to find the constraint force $\boldsymbol{\tau}_{L,i}$. Note that as the suspension is done in the vehicle Centre of Gravity (CoG), the attitude dynamics are unaffected. Define the concatenated vectors $\mathbf{p}$, $\mathbf{v}$ and $\boldsymbol{\tau}_L$ as

$$\mathbf{p} := \begin{bmatrix} \mathbf{p}_1 \\ \mathbf{p}_2 \\ \vdots \\ \mathbf{p}_N \\ \mathbf{p}_l \end{bmatrix}, \quad \mathbf{v} = \begin{bmatrix} \mathbf{v}_1 \\ \mathbf{v}_2 \\ \vdots \\ \mathbf{v}_N \\ \dot{\mathbf{p}}_l \end{bmatrix} \quad \boldsymbol{\tau}_L = \begin{bmatrix} \boldsymbol{\tau}_{L,1} \\ \boldsymbol{\tau}_{L,2} \\ \vdots \\ \boldsymbol{\tau}_{L,N} \\ \boldsymbol{\tau}_l \end{bmatrix} \tag{7}$$

where $\boldsymbol{\tau}_l = -\sum_{i=0}^{N} \boldsymbol{\tau}_{L,i}$

Consider wire i, connecting multirotor i and the load. The line along the wire is given by

$$\mathbf{L}^n_i = \mathbf{p}_i - \mathbf{p}_l \tag{8}$$

A constraint g_i acting on each body is now given by

$$g_i = ||\mathbf{L}_i||^2 - d_i^2 = 0 \tag{9}$$

where d_i is the nominal length of wire i. It's derivatives are given by

$$\dot{g}_i = 2\dot{\mathbf{L}}_i^{\mathrm{T}}\mathbf{L}_i \tag{10}$$

$$\ddot{g}_i = 2\ddot{\mathbf{L}}_i^{\mathrm{T}}\mathbf{L}_i + 2\dot{\mathbf{L}}_i^{\mathrm{T}}\dot{\mathbf{L}}_i = 0 \tag{11}$$

The constraint (11) can now be formulated in the standard form:

$$\mathbf{A}_i(\mathbf{p}, \mathbf{v})\dot{\mathbf{v}} = \mathbf{b}_i(\mathbf{p}, \mathbf{v}) \tag{12}$$

where

$$\mathbf{A}_i = 2\mathbf{L}_i^{\mathrm{T}} \begin{bmatrix} \mathbf{0}_{3\times 3(i-1)} & \mathbf{R}_{b,i}^n & \mathbf{0}_{3\times 3(N-i)} & -\mathbf{I} \end{bmatrix} \tag{13}$$

and

$$\begin{aligned} \mathbf{b}_i = &- 2\mathbf{L}_i^{\mathrm{T}}(\mathbf{R}_{b,i}^n \mathbf{S}(\boldsymbol{\omega}_{b,i})\mathbf{v}_i - \dot{\mathbf{p}}_l) \\ &- \dot{\mathbf{L}}_i^{\mathrm{T}} \dot{\mathbf{L}}_i \end{aligned} \tag{14}$$

According to [17], the constraint force $\boldsymbol{\tau}_L$ are now given by:

$$\boldsymbol{\tau}_L = \mathbf{M}^{1/2}(\mathbf{A}\mathbf{M}^{-1/2})^{+}(\mathbf{b} - \mathbf{A}\dot{\mathbf{v}}) \tag{15}$$

where $\mathbf{M}$, $\mathbf{A}$ and $\mathbf{b}$ are concatenations of $\mathbf{M}_i, \mathbf{A}_i$ and $\mathbf{b}_i$, respectively, and $(\cdot)^{+}$ denotes the More-Penrose Pseudo inverse.

IV. Control Design

In this section, a path following controller for each UAV is designed. For notational simplicity, we skip the subscript i in this part, and it is understood that this concerns each single UAV.

Low-level control of multirotors has been extensively studied in the past, see e.g. [18] for a good review of recent advances. Thus, in this paper we consider the case when each UAV is equipped with a low-level controller, handling attitude control. That is, there exists a control law for $\boldsymbol{\tau}_M$ that takes input desired roll and pitch angle, along with a desired yaw rate r. In addition, as described in [18], an algorithm is embedded in the low-level controller that translates between a desired force $\boldsymbol{\tau}$ in $\{b_i\}$ and attitude, thus giving the following dynamics:

$$\dot{\mathbf{p}} = \mathbf{R}(\psi)\mathbf{v} \tag{16}$$

$$\dot{\psi} = r \tag{17}$$

$$\mathbf{M}\dot{\mathbf{v}} + \mathbf{D}\mathbf{v} + \mathbf{g} = \boldsymbol{\tau} + \boldsymbol{\tau}_L \tag{18}$$

where $\mathbf{D} > 0$ and the term $\mathbf{D}\mathbf{v}$ represents air drag at low speeds, $\mathbf{R}(\psi)$ is a principal rotation about the $\{n\}$ z-axis, and control inputs $\mathbf{u} = [\boldsymbol{\tau}\ r]^{\mathrm{T}}$.

A. Path following controller

This section will synthesize a path-following controller for the system from the previous section. Let $\mathbf{p}_d(\gamma)$ be a desired path in $\mathbb{R}^3$ to follow, and ψ_d a corresponding desired yaw angle. Define the error variables as:

$$\mathbf{z}_1 := \mathbf{p} - \mathbf{p}_d(\gamma) \tag{19}$$

$$z_\psi := \psi - \psi_d(\gamma) \tag{20}$$

whose derivatives are

$$\dot{\mathbf{z}}_1 = \mathbf{R}(\psi)\mathbf{v} - \mathbf{p}_d^{\gamma}(\gamma)\dot{\gamma} \tag{21}$$

$$\dot{z}_\psi = r - \psi_d^{\gamma}(\gamma)\dot{\gamma} \tag{22}$$

Next, define the along-track speed error as:

$$\eta := \dot{\gamma} - v_L(\gamma(t), t) \tag{23}$$

where v_L is a mission velocity known to all vehicles. Thus,

$$\dot{\mathbf{z}}_1 = \mathbf{R}(\psi)\mathbf{v} - \mathbf{p}_d^{\gamma}(\gamma)v_L(\gamma(t), t) - \mathbf{p}_d^{\gamma}(\gamma)\eta \tag{24}$$

$$\dot{z}_\psi = r - \psi_d^{\gamma}(\gamma)v_L(\gamma(t), t) + \psi_d^{\gamma}(\gamma)\eta \tag{25}$$

For notational simplicity, we will drop the arguments on v_L and the reference signals $\mathbf{p}_d$ and ψ_d. Further, define the virtual control $\boldsymbol{\alpha}$ as

$$\mathbf{z}_2 := \mathbf{v} - \boldsymbol{\alpha} \tag{26}$$

which gives

$$\mathbf{M}\dot{\mathbf{z}}_2 = \boldsymbol{\tau} + \boldsymbol{\tau}_L - \mathbf{g} - \mathbf{D}\mathbf{v} - \mathbf{M}\dot{\boldsymbol{\alpha}} \tag{27}$$

B. Step 1

Let a Control Lyapunov Function (CLF) be

$$V_1(\mathbf{z}_1, z_\psi) = \frac{1}{2}\mathbf{z}_1^{\mathrm{T}}\mathbf{z}_1 + \frac{1}{2}z_\psi^2 \tag{28}$$

whose derivative along the solutions are

$$\begin{aligned} \dot{V}_1 = &\mathbf{z}_1^{\mathrm{T}}(\mathbf{R}(\psi)\mathbf{z}_2 + \mathbf{R}(\psi)\boldsymbol{\alpha} - \mathbf{p}_d^{\gamma}v_L - \mathbf{p}_d^{\gamma}\eta) \\ &+ z_\psi(r - \psi_d^{\gamma}v_L + \psi_d^{\gamma}\eta) \end{aligned} \tag{29}$$

Next, choose the virtual control and yaw reference as

$$\mathbf{R}(\psi)\boldsymbol{\alpha} = -\mathbf{K}_p\mathbf{z}_1 + \mathbf{p}_d^{\gamma}v_L \tag{30}$$

$$r = -k_\psi z_\psi + \psi_d^{\gamma}v_L \tag{31}$$

which gives

$$\dot{V}_1 = -\mathbf{z}_1^{\mathrm{T}}\mathbf{K}_p\mathbf{z}_1 - k_\psi z_\psi^2 + \mathbf{z}_1^{\mathrm{T}}\mathbf{R}(\psi)\mathbf{z}_2 + h_1\eta \tag{32}$$

where

$$h_1 = -\mathbf{z}_1^{\mathrm{T}}\mathbf{p}_d^{\gamma} - z_\psi\psi_d^{\gamma} \tag{33}$$

C. Step 2

Let

$$V_2(\mathbf{z}_1, z_\psi, \mathbf{z}_2) = V_1 + \frac{1}{2}\mathbf{z}_2^{\mathrm{T}}\mathbf{M}\mathbf{z}_2 \tag{34}$$

whose derivative is

$$\begin{aligned} \dot{V}_2 = &- \mathbf{z}_1^{\mathrm{T}}\mathbf{K}_p\mathbf{z}_1 - k_\psi z_\psi^2 \\ &+ \mathbf{z}_2^{\mathrm{T}}(\mathbf{R}(\psi)\mathbf{z}_1 + \boldsymbol{\tau} + \boldsymbol{\tau}_L - \mathbf{D}\mathbf{v} - \mathbf{g} - \mathbf{M}\dot{\boldsymbol{\alpha}}) \\ &+ h_1\eta \end{aligned} \tag{35}$$

We can express $\dot{\boldsymbol{\alpha}}$ as

$$\dot{\boldsymbol{\alpha}} = \dot{\bar{\boldsymbol{\alpha}}} + h_2\eta \tag{36}$$

where

$$\begin{aligned} \dot{\bar{\boldsymbol{\alpha}}} = &(-\mathbf{S}(r)\mathbf{R}^{\mathrm{T}}\mathbf{p}_d^{\gamma} + \mathbf{R}^{\mathrm{T}}\mathbf{p}_d^{\gamma^2}v_L + \mathbf{R}^{\mathrm{T}}\mathbf{p}^{\gamma}v_L^{\gamma})v_L \\ &+ \mathbf{S}(r)\mathbf{R}^{\mathrm{T}}\mathbf{K}_p\mathbf{z}_1 - \mathbf{R}^{\mathrm{T}}\mathbf{K}_p\mathbf{R}\mathbf{z}_2 + \mathbf{R}^{\mathrm{T}}\mathbf{K}_p\mathbf{K}_p\mathbf{z}_1 \end{aligned} \tag{37}$$

$$h_2 = \mathbf{R}^{\mathrm{T}}\mathbf{p}_d^{\gamma^2} + \mathbf{R}^{\mathrm{T}}\mathbf{p}_d^{\gamma}v_L^{\gamma} + \mathbf{R}^{\mathrm{T}}\mathbf{K}_p\mathbf{p}^{\gamma} \tag{38}$$

Assuming we know τ_L, let the control $\boldsymbol{\tau}$ be

$$\boldsymbol{\tau} = - \boldsymbol{\tau}_L - \mathbf{R}(\psi)\mathbf{z}_1 + \mathbf{D}\boldsymbol{\alpha} + \mathbf{g} + \mathbf{M}\dot{\bar{\boldsymbol{\alpha}}} - \mathbf{K}_d\mathbf{z}_2 \tag{39}$$

which gives

$$\dot{V}_2 = -\mathbf{z}_1^{\mathrm{T}}\mathbf{K}_p\mathbf{z}_1 - k_\psi z_\psi^2 - \mathbf{z}_2^{\mathrm{T}}\mathbf{K}_d\mathbf{z}_2 - \mathbf{z}_2 D\mathbf{z}_2 + h_3\eta \quad (40)$$

where

$$h_3 = h_1 - \mathbf{z}_2^{\mathrm{T}}\mathbf{M}h_2. \quad (41)$$

D. Step 3

Finally, consider

$$V_3 = V_2 + \frac{1}{2}\eta^2 \quad (42)$$

which gives

$$\begin{aligned}\dot{V}_3 = &-\mathbf{z}_1^{\mathrm{T}}\mathbf{K}_p\mathbf{z}_1 - k_\psi z_\psi^2 - \mathbf{z}_2^{\mathrm{T}}\mathbf{K}_d\mathbf{z}_2 - \mathbf{z}_2 D\mathbf{z}_2 \\ &+ \eta(\ddot{\gamma} - v_L^\gamma\dot{\gamma} + h_3)\end{aligned} \quad (43)$$

where we have used the fact that $\dot{\eta} = \ddot{\gamma} - v_L^\gamma\dot{\gamma}$. Inspired by [12], we chose $\ddot{\gamma}$ as

$$\ddot{\gamma} = -k_\eta\eta + h_3 + v_L^\gamma\dot{\gamma} + \tilde{v} \quad (44)$$

which leads to

$$\dot{V}_3 = -\mathbf{z}_1^{\mathrm{T}}\mathbf{K}_p\mathbf{z}_1 - k_\psi z_\psi^2 - \mathbf{z}_2^{\mathrm{T}}\mathbf{K}_d\mathbf{z}_2 - \mathbf{z}_2 D\mathbf{z}_2 - k_\eta\eta^2 + \eta\tilde{v} \quad (45)$$

We are now ready to state the main result of this section.

Theorem 1. *The controllers given by* (39) *and* (44) *robustly solves the path-following problem. The closed-loop state, including the path following error* $|\mathbf{p} - \mathbf{p}_d|$ *and the speed error* $|\dot{\gamma}_i - v_L(\gamma_i)|$ *are bounded and* input-to-state stable *(ISS) from an input* $\tilde{v}$.

Proof. By applying Youngs Inequality to (45), one can show that there exists $\lambda, \rho > 0$ s.t.

$$\dot{V}_3 \leq -\lambda V_3 + \rho|\tilde{v}|. \quad (46)$$

Further, the zero-equilibrium of the unforced system ($\tilde{v} = 0$) is globally exponentially stable according to [19, Th. 4.10], and by direct application of [19, Th. 4.19] the system is ISS from input $\tilde{v}$.

□

The path-following controller here ensures that a single vehicle will follow a path $p_d(\gamma)$ along a given speed profile $v_L(\gamma)$.

V. Coordination Controller

The coordination controller utilizes graph theory to represent communication links, and a brief introduction is given here.

Let $\mathcal{G}(\mathcal{V}, \mathcal{E})$ be a graph representing the interconnections of the vehicles in the networks. The set of nodes $\mathcal{V}$ represents a vehicle, while the set of edges $\mathcal{E}$ is a bidirectional communication link. Nodes i and j is *adjacent* if an edge exists between them. A graph $\mathcal{G}$ is said to be *connected* if there exists a path between every two nodes in the graph. Let N_i be the set of edges originating in node i. The adjacency matrix A is a square matrix with rows and columns indexed by the nodes such that the i, j-entry of A is defined by

$$A_{i,j} = \begin{cases} 1 & \text{if } j \in N_i \\ 0 & \text{if } j \notin N_i \end{cases} \quad (47)$$

Further, the degree matrix D of a graph is a diagonal matrix of the cardionality of $\mathcal{G}$, that is

$$D_{i,i} = |N_i| \quad (48)$$

The laplacian L of a graph is defined as $L := D - A$. As an example, consider the case where a graph consists of three nodes, all connected to each other. This is a graph with three nodes and three edges, and can be represented by

$$A = \begin{bmatrix} 0 & 1 & 1 \\ 1 & 0 & 1 \\ 1 & 1 & 0 \end{bmatrix}, \; D = \begin{bmatrix} 2 & 0 & 0 \\ 0 & 2 & 0 \\ 0 & 0 & 2 \end{bmatrix} \quad (49)$$

A. Coordination

Now, let the n multirotors be connected by a bi-directional communication link. Let $\mathcal{G}$ be the the graph describing the connectivity map, and L its laplacian matrix. We assume that the graph $\mathcal{G}$ is *connected*. Since the update law (44) has the same structure as introduced in [13], and the path-following controller is ISS by Theorem 1, we apply [12, Theorem 3] to solve the overall CPF problem.

Lemma 1. *By applying the distributed feedback law*

$$\tilde{\mathbf{v}} = -\mathbf{K}_1 L\dot{\boldsymbol{\gamma}} - \mathbf{K}_2(\dot{\boldsymbol{\gamma}} - v_L\mathbf{1} + \mathbf{K}_1 L\boldsymbol{\gamma}) \quad (50)$$

where $\tilde{\mathbf{v}} := [\tilde{v}_i]_{i\in\mathcal{I}}$, $\boldsymbol{\gamma} := [\gamma_i]_{i\in\mathcal{I}}$, $\dot{\boldsymbol{\gamma}} := [\dot{\gamma}_i]_{i\in\mathcal{I}}$, $\mathbf{K}_1, \mathbf{K}_2$ *are positive diagonal matrices, and given sufficiently large path-following gains or coordination gains, the overall closed-loop system consisting of the path following error* $[\mathbf{z}_{1_i}]_{i\in\mathcal{I}}$, *coordination error* $[\gamma_i - \gamma_j]_{i\in\mathcal{I}, j\in N_i}$ *and speed error are* Input-Output-practically Stable *(IOpS).*

Sketch of proof. Direct application of [12, Theorem 3] for continuous communication. The proof involves showing IOpS for the coordination error subsystem, and further application of the small-gain theorem for the interconnected system with the path-following controller. □

VI. Path Generation

This section illustrates how a path can be generated for each UAV, to ensure that the inter-vehicle formation is kept. In addition, the formation is designed in such a way as to minimize the difference of the load drag among each multirotor. There are two parts of this path generation. The first part describes how each vehicle i should be located within the formation. The second describes how the entire formation should rotate as the load traverses the path.

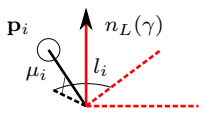

Fig. 2. $\{l\}$-frame. The position $\mathbf{p}_i$ of each multirotor is parameterized by μ_i and l_i.

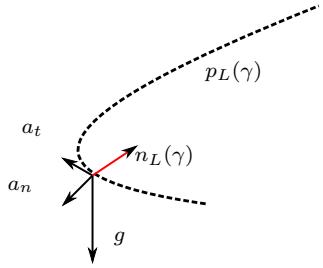

Fig. 3. Along-path frame. Here, a_t is along-path acceleration, a_n the normal component of the acceleration, and g is influence on gravity.

First, consider a load-centered load frame $\{l\}$. The orientation of this frame will be designed later, but this frame moves along a desired load path $\mathbf{p}_L(\gamma)$. Each UAV should follow a path that has a fixed offset in this frame, parameterized by two consecutive rotations l_i and μ_i about the load frame z and y axis, respectively (See Figure 2). Thus, each vehicle position in $\{l\}$ is given by

$$\rho_i^l := \mathbf{R}_z(l_i)\mathbf{R}_y(\mu_i)\begin{bmatrix} L_i \\ 0 \\ 0 \end{bmatrix} \tag{51}$$

where $\mathbf{R}_\alpha(\cdot)$ is a principal rotation about an axis $\alpha \in \{x, y, z\}$, and L_i is the nominal length of wire i. Next, we describe the $\{l\}$ frame. Let $n_L(\gamma)$ be a unit vector that is designed to be parallel and in opposite direction to the total acceleration of the load as it travels along $\mathbf{p}_L(\gamma)$, as in Figure 3. In addition, we require that the frame rotates along the tangential angle of the path. Let $\mathbf{R}_l^n \in \mathcal{SO}^3$ describing the orientation of $\{l\}$ with respect to $\{n\}$ be parameterized by three consecutive rotations ψ_L, ϕ_L and θ_L:

$$\mathbf{R}_l^n(\Theta_L(\gamma)) := \mathbf{R}_z(\psi_L)\mathbf{R}_x(\phi_L)\mathbf{R}_y(\theta_L) \tag{52}$$

where $\Theta_L := [\theta_L, \phi_L, \psi_L]^{\mathrm{T}}$ and

$$\psi_d(\gamma) = \operatorname{atan2}(\mathbf{p}_{L,y}^\gamma, \mathbf{p}_{L,x}^\gamma) \tag{53}$$

$$\phi_L(\gamma) = \arctan\frac{\kappa(\gamma)v_L^2(\gamma)}{g} \tag{54}$$

$$\theta_L(\gamma) = \arctan\frac{v_L^\gamma(\gamma)}{g} \tag{55}$$

in which we require the path $\mathbf{p}_L(\gamma)$ to be parameterized by its path length, $v_L(\gamma)$ is the speed profile along the path and $\kappa(\gamma)$ is the curvature.

The path of UAV i can thus be calculated from:

$$\mathbf{p}_i(\gamma) = \mathbf{p}_L(\gamma) + \mathbf{R}_l^n(\gamma)\rho_i^l \tag{56}$$

Remark 1. *Note that the first and second derivatives of $\mathbf{p}_{d,i}$ are required for path-following, which results in large and computationally expensive expressions. Depending on application, practical simplification such as assuming slowly varying speed reference v_L so we have $v_L^{\gamma^2} \approx 0 \to [\phi_L^{\gamma^2}, \theta_L^{\gamma^2}] \approx 0$ will greatly simplify the computations.*

VII. Speed Profile

In addition to the spatial path introduced above, a speed profile to be tracked while the vehicles traverse the path is needed. The speed-profile should be C^2 continuous and provide smooth velocity signals. In this paper, we utilize a fifth order polynomial represented by Bernstein polynomials [20]. Further, we have four distinct phases, characterized by acceleration, constant speed, deceleration and stop, respectively. In the following, we will the describe how to compute $v_L(\gamma)$ and its derivatives in the acceleration phase. In the constant speed and stop phase, the values are trivial. The speed profile in the deceleration phase is computed in a similar manner as in the acceleration phase.

The acceleration phase is characterized by an initial speed V_0, a desired final speed V_f, and a rise time T (that is, $v_L(0) = V_0$ and $v_L(T) = V_f$). *Note that when combining the speed profile with a spatial path, T will be a certain value of the path parameterization γ, that is, a speed at a certain point on the path.* Then, we have

$$v_L(\gamma) = \sum_{k=0}^{2} V_0 b_k^5(\frac{\gamma}{T}) + \sum_{k=3}^{5} V_f b_k^5(\frac{\gamma}{T}) \tag{57}$$

where b_k^5 is the fifth-order Bernstein basis defined by [20]:

$$b_k^n(\tau) = \binom{n}{k}(1-\tau)^{n-k}\tau^k \text{ for } k = 0, \ldots, n \tag{58}$$

It's derivatives are readily given by

$$\frac{\partial v_L}{\partial \gamma} = \frac{5}{T}(V_f - V_0)b_2^4(\frac{\gamma}{T}) \tag{59}$$

$$\frac{\partial^2 v_L}{\partial \gamma^2} = \frac{20}{T^2}(V_f - V_0)(b_1^3(\frac{\gamma}{T}) - b_2^3(\frac{\gamma}{T})) \tag{60}$$

An example of a complete speed profile is given in Figure 4. Here, we have an initial speed of $v_L(0) = 1$, and require that $v_L(3) = 4$. The deceleration phase starts at $\gamma = 7$, before we have a stop at $\gamma = 10$.

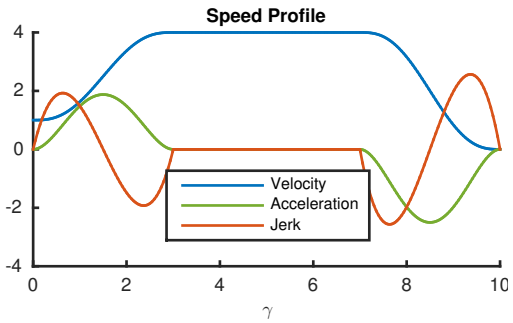

Fig. 4. An example speed profile during acceleration, constant speed and deceleration phase.

VIII. Simulation Study

In this section, we apply the controllers developed in this paper to a team of three multirotors transporting a suspended

load along a circular path of radius $R = 10$. The paths for each vehicle is generated as in Section VI, with $\mu_{1,2,3} = 60°$, and $l_1 = 0, l_2 = 120°, l_3 = -120°$. The simulations are conducted with the full nonlinear dynamics, including the constraint force from the payload, as developed in Section III. Further, each UAV is equipped with a low-level attitude controller, as discussed in Section IV. In this simulation, the attitude controller is a simple PD structure. The maximum roll- and pitch-angle have been set to 30 degrees, to force reasonable realistic maneuvers. Each vehicle has a mass $m = 4$kg, transporting a payload of mass $m_L = 1$kg. Further, the speed profile is designed as in Section VII, with a maximum speed of 3 m/s, accelerating from 0.5 m/s at $\gamma_i = 0$ to $\gamma_i = 2R\pi/3$, a third part around the circle. The control parameters was chosen as: $\mathbf{K}_p = 5\mathbf{I}$, $\mathbf{K}_d = 5\mathbf{I}$, $k_\psi = 1$, $k_\eta = 20$, $\mathbf{K}_1 = \mathbf{K}_2 = 30\mathbf{I}$. Integration was conducted by the *Runge-Kutta 4* method, at 100 Hz. Again, note that we assume that each multirotor can measure the drag from the suspended load to cancel it. Realistically, this can be achieved by an angular sensor combined with a force sensor, as demonstrated in [1]. Further, we assume continuous communication links. However, the framework used in this paper can easily be extended using the results in [**?**].

The results of the simulation can be seen in Figures 5–9. In Figure 5, the coordination error is illustrated. Clearly, it is seen that the error quickly converges to zero, and we have achieved coordination. Likewise, the path-following error is depicted in Figure 6 and shows convergence to a neighborhood around zero. The load drag on each multirotor is illustrated in Figure 7, and it is seen that the distribution is relatively uniform, except during the acceleration and deceleration phases. Further, in Figure 8, the total speed of the load as it traverses its path is shown. As can be seen, it reaches its desired speed of 3 m/s. Figure 9 provides snapshots of the simulation as it unfolds.

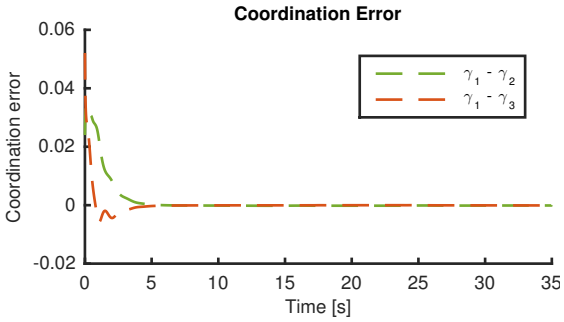

Fig. 5. The coordination error during the simulation.

IX. Conclusions

In this paper, we have designed a cooperative control law to transport a suspended load with a group of coordinating multirotors. The local path-following controller was analyzed by Lyapunov theory, and proven to solve the *path-following* problem. Coordination was achieved by applying results from the literature, most notably [13] and [14]. Further, we

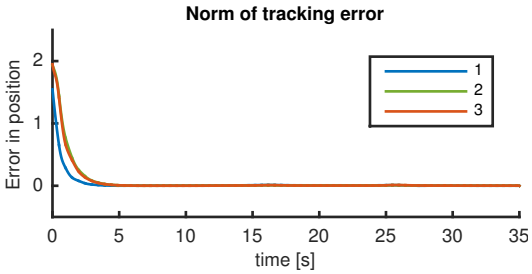

Fig. 6. Path-following error of each multirotor. A small error is induced when the formation changes speed quickly; this is due to the performance of the low-level controllers.

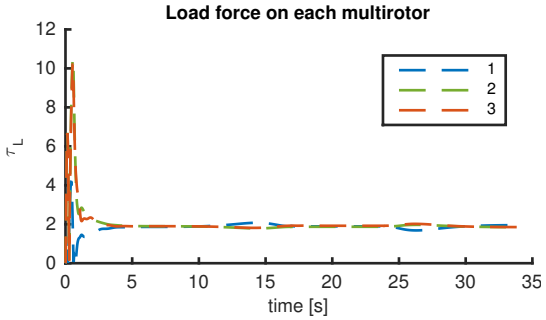

Fig. 7. Load drag on each multirotor. The high initial values are due to initial movements of the vehicles, before they reach synchronization.

illustrated how to generate paths for each vehicle to minimize the variation of load drag among the vehicles to ensure smooth operations. Numerical results verified the results, were we showed convergence of the path-following- and coordination error. Our suggested methodology to minimize the load variation showed decent results, but future work will look at improving this. Further, robustness-properties with respect to external disturbances needs further investigation.

References

[1] M. Bernard and K. Kondak, "Generic slung load transportation system using small size helicopters," *2009 IEEE International Conference on Robotics and Automation*, pp. 3258–3264, May 2009.

[2] J. Fink, N. Michael, S. Kim, and V. Kumar, "Planning and control for cooperative manipulation and transportation with aerial robots," *The International Journal of Robotics Research*, vol. 30, no. 3, pp. 324–334, Sept. 2010.

[3] T. Lee, "Geometric Control of Multiple Quadrotor UAVs Transporting a Cable-Suspended Rigid Body," in *53rd Conference on Decision and Control*, 2014.

[4] W. R. W. Ren, R. Beard, and E. Atkins, "A survey of consensus problems in multi-agent coordination," *Proceedings of the 2005, American Control Conference, 2005.*, pp. 1859–1864, 2005.

[5] M. Arcak, "Passivity as a Design Tool for Group Coordination," *IEEE Transactions on Automatic Control*, vol. 52, no. 8, pp. 1380–1390, 2007.

[6] H. Bai, M. Arcak, and J. T. Wen, *Cooperative control design: A systematic, passivity-based approach*, 2011.

[7] K. Y. Pettersen, J. T. Gravdahl, and H. Nijmeijer, *Group Coordination and Cooperative Control*. Springer Berlin Heidelberg, 2006.

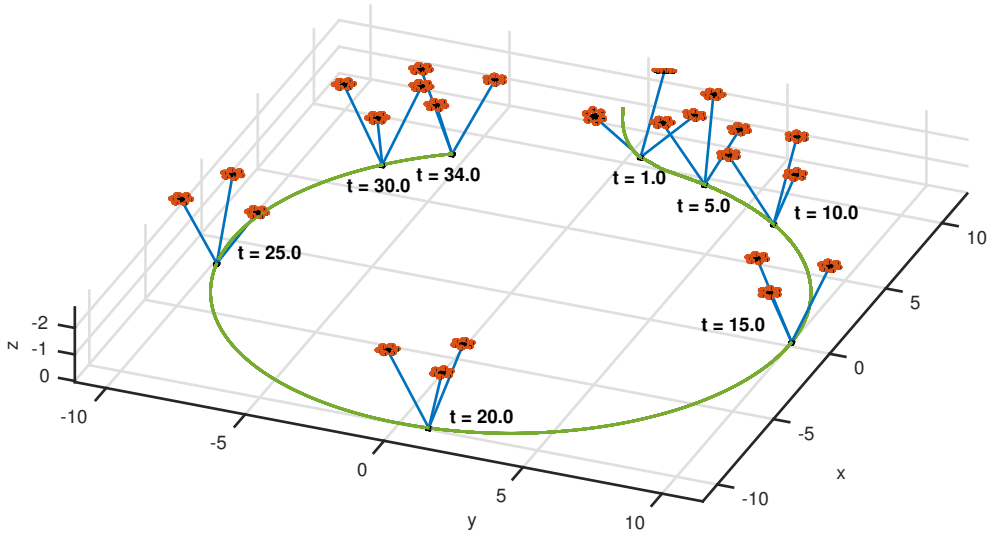

Fig. 9. Snapshots of the simulation at different times, as marked in the figure. As can be seen, the multirotors achieve their desired formations.

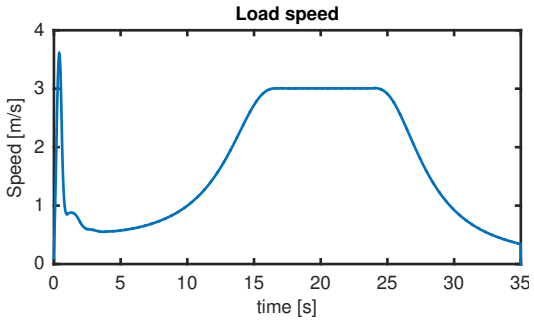

Fig. 8. The total speed of the suspended load. As can be seen, it reaches it designated max speed at 3 m/s, before decelerating during the end of the circle movement.

[8] R. Skjetne, I. Ihle, and T. I. Fossen., "Formation Control by Synchronizing multiple maneuvering systems," in *Proc. of the IFAC MCMC'03*, 2003.

[9] R. Skjetne, T. I. Fossen, and P. V. Kokotović, "Robust output maneuvering for a class of nonlinear systems," *Automatica*, vol. 40, no. 3, pp. 373–383, Mar. 2004.

[10] J. Hauser and R. Hindman, "Aggressive flight maneuvers," in *Proceedings of the 36th IEEE Conference on Decision and Control*, vol. 5, no. December, 1997, pp. 86–91.

[11] J. Fax and R. Murray, "Information Flow and Cooperative Control of Vehicle Formations," *IEEE Transactions on Automatic Control*, vol. 49, no. 9, pp. 1465–1476, Sept. 2004.

[12] A. P. Aguiar and R. Ghabcheloo, "Coordinated Path-Following Control of Multiple Autonomous Underwater Vehicles," in *International Offshore and Polar Engineering Conference*. Lisbon, Portugal: International Society of Offshore and Polar Engineers, 2007, pp. 4345 – 4350.

[13] A. P. Aguiar and A. M. Pascoal, "Coordinated path-following control for nonlinear systems with logic-based communication," *Proceedings of the IEEE Conference on Decision and Control*, pp. 1473–1479, 2007.

[14] R. Ghabcheloo, a. P. Aguiar, a. Pascoal, C. Silvestre, I. Kaminer, and J. Hespanha, "Coordinated Path-Following in the Presence of Communication Losses and Time Delays," *SIAM Journal on Control and Optimization*, vol. 48, pp. 234–265, 2009.

[15] F. E. Udwadia, "Equations of motion for mechanical systems: A unified approach," *Journal of Non-linear Mechanics*, vol. 31, no. 6, pp. 951–958, 1996.

[16] M. Bisgaard, "Modeling, Estimation, and Control of Helicopter Slung Load System," Ph.D. dissertation, Aalborg University, 2008.

[17] F. E. Udwadia and P. Phohomsiri, "Explicit Poincaré equations of motion for general constrained systems. Part I. Analytical results," *Proceedings of the Royal Society A: Mathematical, Physical and Engineering Sciences*, vol. 463, no. 2082, pp. 1421–1434, June 2007.

[18] R. Mahony, V. Kumar, and P. Corke, "Modeling, Estimation, and Control of Quadrotor," *IEEE Robotics & Automation magazine*, vol. 19, no. 3, pp. 20–32, Sept. 2012.

[19] H. K. Khalil, *Nonlinear Systems*, 3rd ed. Prenctice Hall, 2002.

[20] R. T. Farouki, *Pythagorean-Hodograph Curves: Algebra and Geometry Inseparable*. Springer Berlin Heidelberg, Jan. 2008, vol. 2, no. 1.